

UNCLASSIFIED

**Defense Technical Information Center
Compilation Part Notice**

ADP010642

**TITLE: Fatigue Substantiation and Damage
Tolerance Evaluation of Fiber Composite
Helicopter Components**

DISTRIBUTION: Approved for public release, distribution unlimited

This paper is part of the following report:

**TITLE: Application of Damage Tolerance Principles
for Improved Airworthiness of Rotorcraft
[l'Application des principes de la tolerance a
l'endommagement pour une meilleure aptitude au
vol des aeronefs a voilure tournante]**

To order the complete compilation report, use: ADA389234

The component part is provided here to allow users access to individually authored sections of proceedings, annals, symposia, ect. However, the component should be considered within the context of the overall compilation report and not as a stand-alone technical report.

The following component part numbers comprise the compilation report:

ADP010634 thru ADP010648

UNCLASSIFIED

Fatigue Substantiation and Damage Tolerance Evaluation of Fiber Composite Helicopter Components

H. Bansemir, S. Emmerling
Eurocopter Deutschland GmbH
81663 München, Germany

ECD-0026-99-PUB

ABSTRACT

Helicopter rotor systems are dynamically loaded structures with many composite components such as main and tail rotor blades and rotor hubs. The new civil helicopter EC135 has a bearingless main rotor system certified according to the 'Special Condition for Primary Structures Designed with Composite Material' of the German airworthiness authority LBA containing increased safety demands. This special condition addresses subjects like

- demonstration of ultimate load capacity including consideration of manufacturing and impact damages
- fatigue evaluation for parts suitable or unsuitable for damage tolerance method and the related inspection procedures
- investigation of growth rate of damages that may occur from fatigue, corrosion, intrinsic and manufacturing defects or damages from discrete sources under repeated loads expected in service
- residual strength requirements
- consideration of the effects of material variability and environmental conditions like hot/wet strength degradation etc.
- substantiation of bonded joints

The fatigue tolerance evaluation and damage tolerance substantiation for composite structures are shown in this paper. The fulfillment of the 'Special Conditions' is demonstrated for the main rotor blade of the EC135.

TABLE OF CONTENTS

1. INTRODUCTION
2. DYNAMICALLY LOADED ROTOR BLADES
3. QUALITY ASSURANCE METHODS APPLIED FOR COMPOSITE ROTOR BLADES
4. GENERAL CERTIFICATION REQUIREMENTS AND SUBSTANTIATION PRINCIPLES
5. ESTABLISHMENT OF BASIC MATERIAL FATIGUE AND DAMAGE TOLERANCE DATA
6. BASIC STRUCTURAL BEHAVIOUR
7. DYNAMIC STRENGTH COMPONENT TESTING AND DEMONSTRATION OF LIMIT LOAD CAPACITY
8. SUMMARY

1. INTRODUCTION

In 1967 the BO105, a product of the former helicopter division of MBB, now Eurocopter Deutschland, flew for the first time. Three years later this light twin helicopter was certified by the German Luftfahrtbundesamt (LBA). Up to now almost 1500 BO105 multipurpose helicopters have been manufactured and are flying in more than 40 countries. The worldwide first serial hingeless main rotor system was a key element of this helicopter, using the advantages of the newly developed fiber glass

technology. Thus the flapping and lead-lag hinges could be eliminated. The innovative rotor design included new materials such as titanium for the rotor hub and fiber glass epoxy for the main and tail rotor blades. The substitution of the hinges was a big step towards weight reduction and cost-saving due to the reduction of parts. Another benefit of the rotor system was the improved handling qualities and flight manoeuvrability especially in gusty weather conditions. The pitching motion, however, is still carried out using roller bearings, which require some effort in manufacturing and service.

The first flight of the BK117 of MBB / Kawasaki Heavy Industries took place June 13, 1979. Since that time about 375 helicopters are flying worldwide. The rotor system of this helicopter is identical to the BO105 except the rotor blade design which includes a different geometry but mainly equivalent glass/epoxy and carbon/epoxy composite materials.



Figure 1: The Multi-Purpose Helicopters BO105 and BK117

In 1991/92 Eurocopter started the development of the multi-purpose light twin helicopter EC135. The main rotor was derived from the BO108 technology (Ref. [1-4]), whereas the tailboom with the Fenestron anti-torque system was developed by Eurocopter France. The first prototype carried out its maiden flight in February 1994, powered by two Turbomeca Arrius 2B engines, whereas the second prototype began flight testing two months later, powered by the alternative Pratt & Whitney PW206B engines.

After extensive testing of three prototypes, structures and systems and with the help of validated analysis, the type certification was issued in June 1996 by the LBA and in July 1996 by the DGAC and FAA. Since that date EC135 helicopters with certified basic and optional equipment have been delivered to customers all over the world.

2. DYNAMICALLY LOADED ROTOR BLADES

The basic design features of the multi-mission helicopter EC135, a 3D drawing and the overall dimensions, are shown in Figure 3 and Table 1.



Figure 2: The New Multi-Mission Helicopter EC135

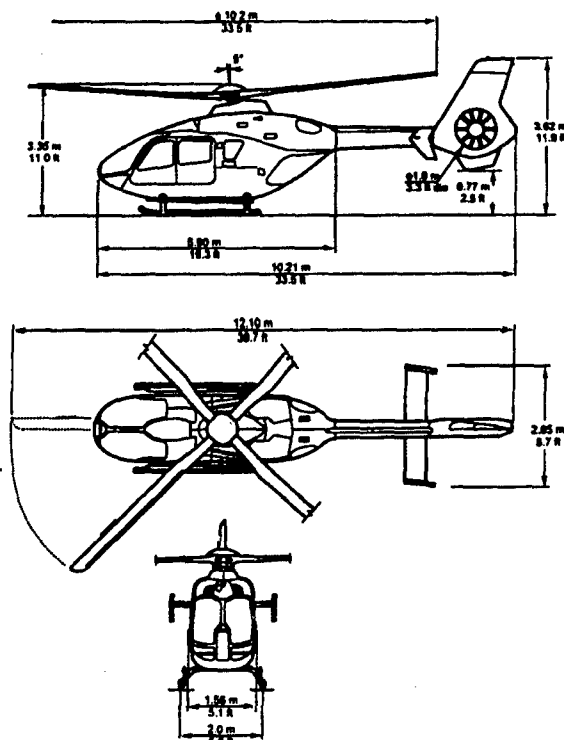


Figure 3: 3D-View Drafting of the EC135

Main emphasis was laid on the design of the dynamic components in order to achieve unlimited life with high flaw tolerance. Thus the direct operating costs can be reduced. Most of the components were designed for on-condition maintenance.

One of the most significant development features of the EC135 is the Bearingless Main Rotor (BMR) shown in Figure 4. The BMR shows a 50 kg weight reduction and 40 % less parts count compared to the BO105 rotor. The fully composite design (fiber glass and graphite epoxy) has characteristic fail safe design features such as a blade root attachment of the flexbeam consisting of two double lugs and a two load path attachment of the tuning masses to the blade. The flexbeam of the BMR shows an equivalent flapping hinge offset of about 9% of the blade radius. The rotor is a soft inplane design. The elastomeric damping devices provide sufficient inplane damping and the system control cuff - flexbeam - control rod produce adequate pitch-lag coupling [4].

Whereas the rotor hub of the EC135 has an exceptionally simple design, the structure of the blade root has become rather complicated as it has to take on the tasks of the hinges and bearings of a conventional rotor. This blade root is also called flexbeam and is the key element of the bearingless rotor.

A skilful design, however, allows the local separation of the different tasks in the flexbeam.

Table 1: Main Characteristics of the EC135 with Arrius 2B1 Engines

Empty Weight of Aircraft	1465 kg	3230 lbs
Max. Take-Off Weight	2720 kg	6000 lbs
MTOW with External Load	2900 kg	6393 lbs
Max. Continuous Power	2x 283 kW	
Take-Off Power	2x 308 kW	
2.5 min OEI	1x 411 kW	
Rotor RPM	100 - 104 %	
Blade Tip Speed	211 - 219 m/s	
Max. Cruising Speed SL ISA	257 km/h	139 kts
Never Exceed Speed SL ISA	278 km/h	150 kts
Hover in Ground Effect	4040 m	13250 ft
Hover Out of Ground Effect	3100 m	10200 ft
Rate of Climb	8.4 m/s	1650 ft/min
Maximum Range	620 km	335 nm
Maximum Endurance	4:33 hrs	

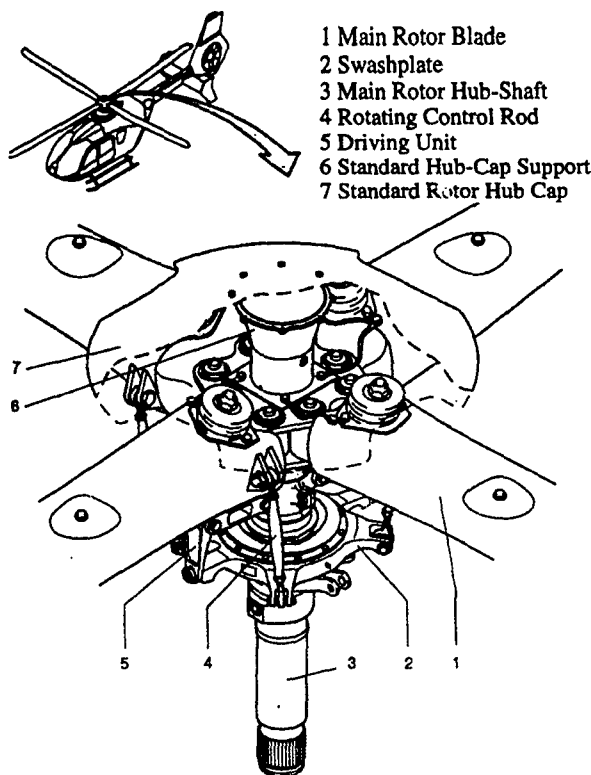


Figure 4: The Bearingless Main Rotor System with Elastomeric Dampers

The blade and its inner part are shown in the Figures 5 and 6. It is a GFRP (glass fiber reinforced plastic) prepreg design using E-Glass and a 120°C epoxy system. It consists of unidirectional tapes orientated in the longitudinal direction. These are mainly responsible for the longitudinal and bending stiffnesses and carry the greatest part of the centrifugal force and the bending moments, whereas the $\pm 45^\circ$ layers in the shear

web and the blade skin have to carry the greatest part of the shear loads including torsional moment.

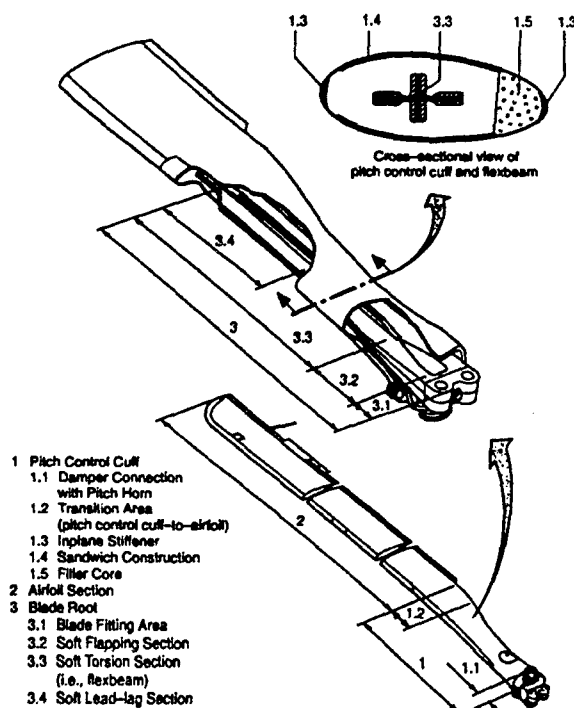


Figure 5: The Blade of the Bearingless EC135 Main Rotor

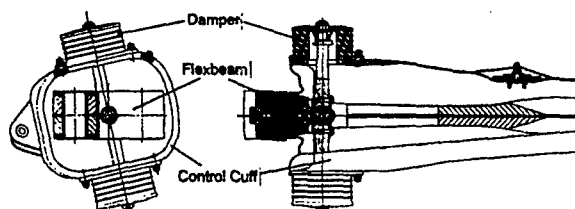


Figure 6: Blade Attachment Area with Control Cuff and Dampers

At radius station $R = 110$ mm the blade is connected with the help of two bolts to the rotor hub. The loads are transferred via two double lugs at the relatively stiff blade attachment area. A tapered transition area leads to the flat 'flapping hinge' section. This section has to allow the flap angles by bending.

In the following transition area the layers are shifted to the cruciform shape of the torsional element. This has a short length of about 0.5 m and replaces the blade bearings. Its slim and deeply slit cruciform cross section results in an extremely low torsional stiffness of the flexbeam of 4.2 Nm° without and of 7.2 Nm° with centrifugal force.

The cruciform shape of the torsional element has special advantages. Warping restriction can be avoided, and the flapping and lead-lag stiffnesses can be tuned independently from each other. In addition the relatively high flapping stiffness of the torsional element reduces the static sag of the non-rotating rotor. Therefore no blade stop is needed.

The total mass of the blade is almost 40 kg including about 7.5 kg of additional masses for the tuning of frequencies and the reduction mainly of the lead-lag bending moments.

These tuning masses are locally built in at several radius stations. Apart from the blade tip mass, they are enclosed by thermoplastic casings. Great care was taken to ensure a fail safe fixation of these masses in the blade structure, as they locally generate high additional centrifugal forces. Each of two separate load paths can completely transfer the loads. Besides large-sized bonding areas being the first load path the masses are completely surrounded by blade structure, lugs, C-profiles etc., so that the centrifugal forces can also be totally carried via form-locking, even if the bonding had failed.

Main emphasis was laid on an excellent fail safe behaviour not only of the tuning masses but also of the complete rotor blade. The following table summarizes some of its characteristic features [3,4].

Table 2: Characteristic Fail Safe Design Features of the EC135 Main Rotor Blade

1. Flexbeam	
- Complete spar including flexbeam manufactured in one shot	
- 2 'double lugs' at the blade attachment	
2. Control Cuff	
- Integral with blade skin	
- Double shear bonding of control cuff halves	
- Form-locking design and double shear bonding of the connection to the pitch lever	
3. Connection Control Cuff and Flexbeam ($R = 1172$ mm)	
- 2 load paths:	a) large bonding areas
	b) form-locking design
4. Tuning Masses	
- 2 load paths:	a) large bonding areas
	b) masses completely enclosed by supporting structures

3. QUALITY ASSURANCE METHODS APPLIED FOR COMPOSITE ROTOR BLADES

At Eurocopter Deutschland computed tomography (CT) is used for the quality assurance of the rotor blades of BO105, BK117 and EC135 [7], see Figure 7 and Figure 8. For the EC135 blades CT was also used during the design phase and has been performed for each blade at the beginning of the serial production.

Originally CT was developed for the medical field. To create a cross section image, an X-ray beam rotates around the object in a complete circle. From several projection directions attenuation profiles of the beam are measured. With these data a computer calculates the image of the cross section slice having the thickness of the X-ray beam of about 1.5 mm. During the rotor blade examination cross section images are produced at various radius stations. When these stations are close together, e.g. in the lug area, vertical and horizontal cuts in radial direction can also be computed.

CT is a very effective non-destructive testing (NDT) method to check the quality of fiber composite parts. Damages or defects like cracks or waves in the laminate of at least 0.2 mm size can be detected. By the determination of special CT numbers the local material density can be established. Thus e.g. it can be checked if dark spots in a cross section consist of resin or critical air inclusions. With the help of CT, the manufacturing quality of the EC135 blade could be improved significantly.

A test specification for the EC135 main rotor blade describes in detail, in which area which kinds of damages are allowed. If a new type of damage occurs seeming to be eventually critical, a component test is performed. This test has to prove, if the damage affects the life of the structure. When it does, this damage is not accepted for the serial blade quality.



Figure 7: Non-Destructive Testing of the BO105/BK117 Attachment Lug Area by Means of Computed Tomography

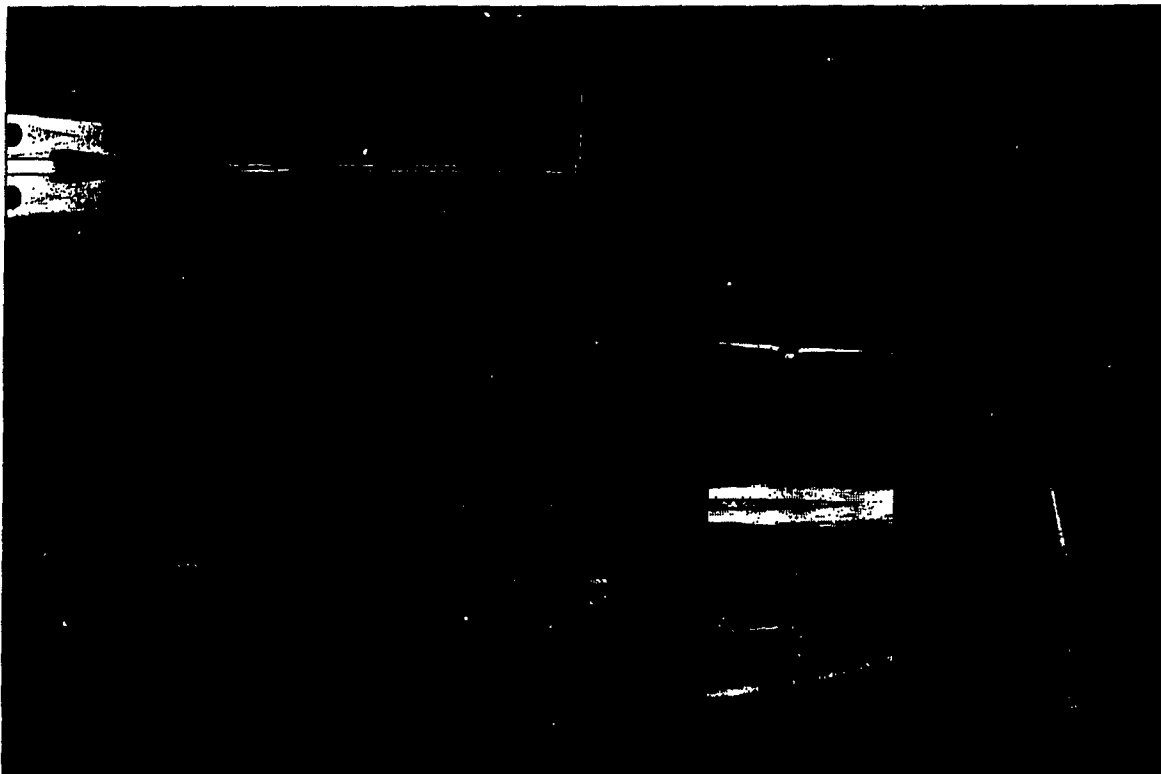


Figure 8: Non-Destructive Testing of the EC135 Main Rotor Blade with Manufacturing Defects at an Early Development Stage by Means of Computed Tomography

4. GENERAL CERTIFICATION REQUIREMENTS AND SUBSTANTIATION PRINCIPLES

The EC135 has been certified according to Joint Aviation Requirements JAR27 'Small Rotorcraft'. However, as the primary structure includes composite materials, the German airworthiness authority Luftfahrtbundesamt issued a Special Condition 'Primary structures designed with composite material' that had to be fulfilled additionally. The special condition addresses subjects like

- demonstration of ultimate load capacity including consideration of manufacturing and impact damages
- investigation of growth rate of damages that may occur from fatigue, corrosion, intrinsic defects, manufacturing

defects or damages from discrete sources under repeated loads expected in service

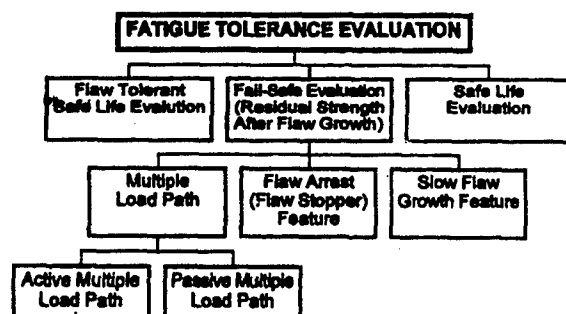
- fatigue evaluation for parts suitable or unsuitable for damage tolerance method and the related inspection procedures
- residual strength requirements
- consideration of the effects of environmental conditions and material variability
- substantiation of bonded joints

In general the fatigue substantiation of dynamically loaded structures is based on the Safe Life procedure. As derived and stated in the Helicopter Fatigue Design Guide (see also [5]), the service life is determined from the usually applied substantiation procedure:

- Establishment of a safe fatigue strength working curve
- Derivation of load spectrum from inflight measurements
- Calculation of the service life by means of Miner's linear damage accumulation hypothesis.

In accordance with the fatigue evaluation of Transport Category Rotorcraft Structures FAR29.571 (Table 3) multiple load paths were established whenever possible.

Table 3: Fatigue Evaluation of Transport Category Rotorcraft Structure (Including Flaw Tolerance) according to FAR29.571



For the dynamically loaded EC135 rotor blade the Flaw-Tolerant Safe Life Method was used for substantiation. In addition fail safe features were incorporated into the design to ensure sufficient residual strength capability after flaw growth. The composite structures were predamaged with the help of impactors up to 25 Joule.

The no-crack-growth ability of the fuselage composite parts was demonstrated by tests.

The rotor blade of the EC135 is an integrated composite structural element with multiple load paths in several areas and for several load cases. In Figure 10 blade sections are shown with the critical load and failure situation. The blade sections with intrinsic, manufacturing and impact damages were tested with dynamic loads. With the help of the performed tests S/N working curves for the flexbeam were established.

The S/N-curve expressed in amplitude values is represented by the following relation:

$$S_A = S_{A_{\infty}} + \frac{S_{A_{ult}} - S_{A_{\infty}}}{\exp\left[\left(\frac{\log(N)}{\alpha}\right)^{\beta}\right]}$$

where $S_{A_{\infty}}$ is the endurance limit, $S_{A_{ult}}$ the ultimate value, N the number of cycles and α , β are the shape parameters for the adjustment of the curve [5].

The S/N-curve for torsion of the flexbeam is shown in Figure 9.

The flight tests yielded the necessary load spectra. A complete spectrum contains the working loads (High-Frequency-Spectrum) and the GAG loads (Ground-Air-Ground-Spectrum). The damage ratios and the resulting lives of the structures were calculated according to Miner's linear damage accumulation hypothesis.

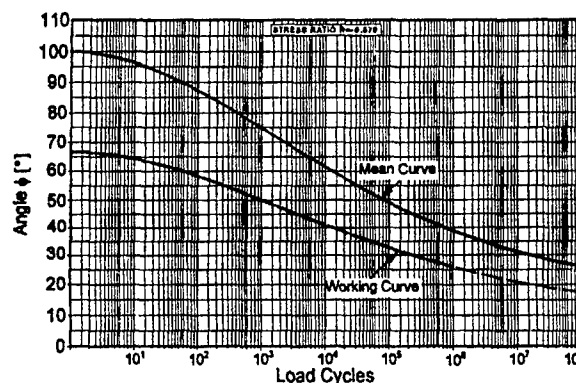


Figure 9: S/N-Curve for Torsional Angle of the Flexbeam

5. ESTABLISHMENT OF BASIC MATERIAL FATIGUE AND DAMAGE TOLERANCE DATA

The material stiffness and strength properties of the fiber composite materials were measured at ECD itself with the help of standardised coupon tests. The basic unidirectional stiffnesses and strengths were determined by long and short beam coupon specimens.

For the static strength substantiation interlaminar failure had to be avoided up to limit load. Up to ultimate load, however, no fiber failure was allowed. The strength degradations due to high temperature and moisture had also to be taken into account. For the fatigue strength substantiation room temperature conditions could be used. For the residual strength test with limit load after fatigue test the hot/wet degradation had to be considered again. As the blade is a fail safe structure, B-values could be taken for the substantiation [8].

Table 4 describes the tested material specimen types, the hot/wet conditions for the EC135 certification and the proceeding for the use of the allowables agreed with the certification authorities.

Table 4: Material Properties and Environmental Conditions

1. Material stiffness and strength properties determined by coupon tests:
 - a) bending specimens (long beam type)
 - b) shear specimens (short beam type)
2. Environmental conditions
 - a) 75°C and 85% relative humidity (hot/wet conditions)
 - b) room temperature conditions for fatigue strength substantiation
3. Allowables for material strength
 - a) Ultimate load and residual strength
 - hot/wet conditions
 - σ_{II} decisive (fiber crack)
 - No interlaminar failure (τ_{ILS}) allowed up to limit load
 - b) Flight loads
 - room temperature conditions
 - B-values for substantiation of blade as fail safe structure

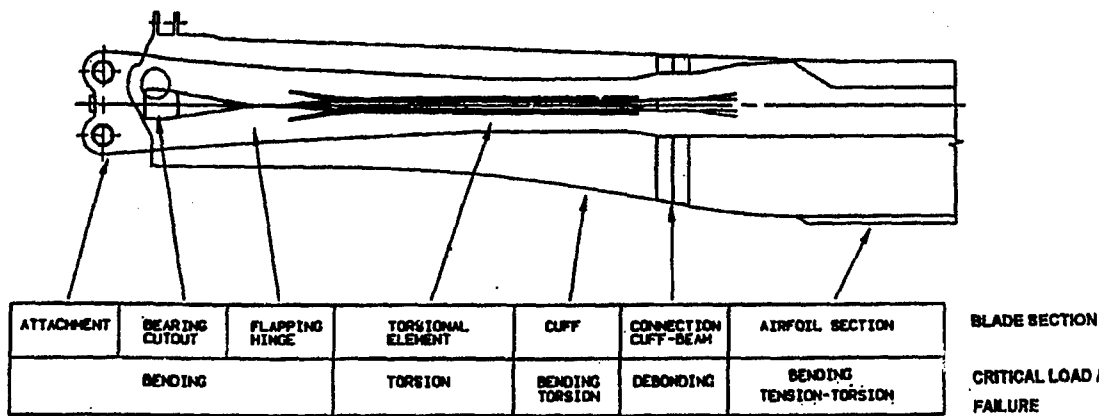


Figure 10: Critical Load / Failure Areas of the EC135 Main Rotor Blade

As seen in Figure 10, the sections of the rotor blade are loaded in different ways. As the rotor blade cannot be tested dynamically as complete structure, several sectional areas were tested according to their critical load and failure behaviour. Thus for each section S/N-curves were derived and transformed to working curves taking into account 99.9 % survivability and 95 % confidence level.

As also seen in Figure 10 the root of the blade is mainly loaded either by bending or by torsion. The failure modes of the blade were established with the help of structural dynamic tests.

Delaminations due to torsional and bending stresses are important failures, which are studied by means of coupons and structural parts. In Figure 11 the three delamination modes I, II, and III are shown. By design the delamination mode I was eliminated if possible. Basic equations for bonded and tapered joints are derived in Figure 11. The relation between the transferable stress σ_{II} and the peak shear stress τ_{max} was analysed by means of the classical shear-lag theory and by fracture mechanics. For bonded joints the fracture mechanic property G_{II} is proportional to thickness of the adhesive and the square of the peak shear stress divided by the shear modulus of the adhesive [8, 9, 10].

To establish experimentally the energy release rates for mode I, mode II and mixed mode I/II a variety of test specimens as shown in Table 5 have been developed [12].

Comparative investigations between the Transverse Crack Tension TCT and End Notch Flexure ENF test configuration [15] showed a much better aptitude of the TCT specimen to indicate the static and dynamic delamination behaviour of unidirectional composites. Compared with the ENF specimen the TCT specimen is less complicated in fabrication and the tests include no shear deformation and no frictional effects which can be observed with the ENF tests. Especially while investigating the crack growth behaviour the TCT test has the advantage of maintaining an energy release rate independent from the crack length which is not true for the ENF tests.

In opposite to the TCT specimen with inner fiber interruption as shown in Table 5 a modified TCT specimen with outer fiber interruption shown in Figure 12 was created to investigate the mixed mode I/II.

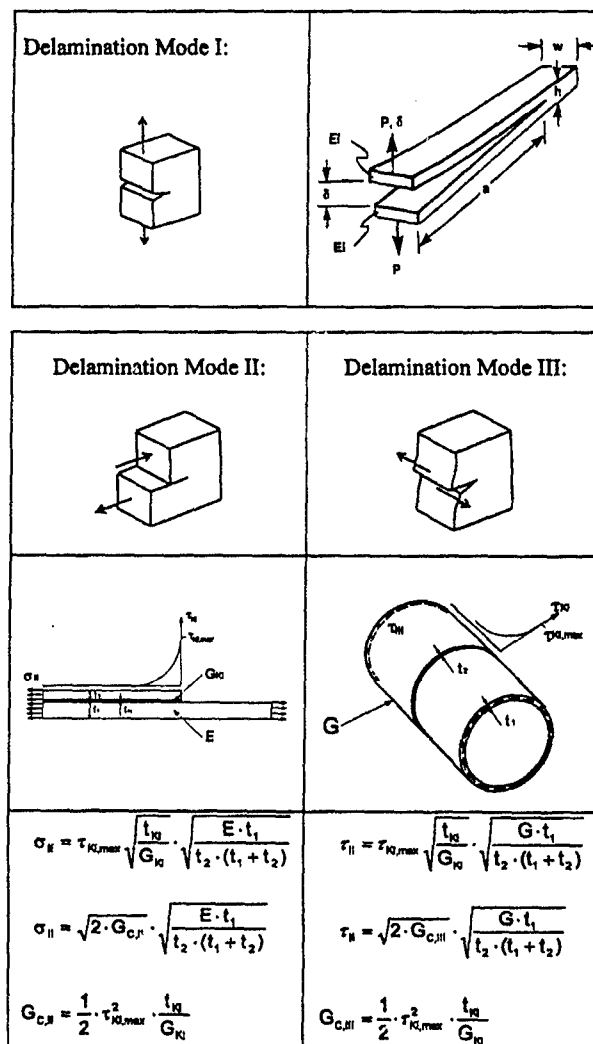


Figure 11: Delamination Modes of Overlaps and Joints and Relevant Delamination Formulas for Mode II and III

Table 5: Tests for Experimental Determination of Energy Release Rates for Mode I, Mode II and Mode I / II

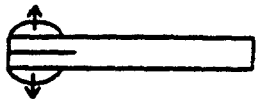
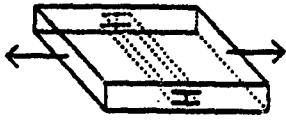
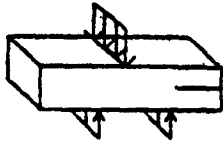
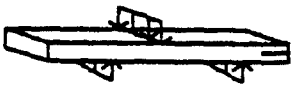
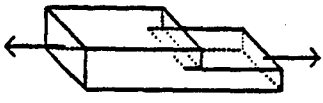
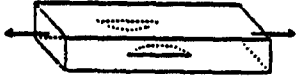


Mode	Sign / Designation	Test Configuration
I	DCB double cantilever beam	
II	TCT transverse crack tension TCT transverse crack tension-compression	
II	SBS short beam shear	
II	ENF end-notched flexure	
I/II	CLS crack lap shear	
I/II	EDT edge delamination tension EDYC edge delamination tension-compression	
I/II	HDT hole delamination tension HDTC hole delamination tension-compression	
I/II	ENT edge notch tension ENTC edge notch tension-compression	



Figure 12: Modified TCT Specimen with Outer Fiber Interruption

For the analysis of delamination initiation and delamination propagation due to dynamic tension loads TCT test specimens with inner and outer fiber interruption shown were used. The test specimen with inner fiber interruption corresponds to the

pure delamination mode II, whereas the specimen with outer fiber interruption takes the influence of mode I on mode II into consideration.

The delamination stress σ_U (upper value) for the stress ratio $R = 0.1$ versus load cycles is shown in Figure 13 for the outer fiber interruption. The specimens for establishment of this curve were fabricated of E-Glass/913 unidirectional prepreg material, which is used for the flexbeam of the EC135 helicopter. The delamination onset curve is described by the four parametric Weibull formula:

$$\sigma = \sigma_{unl} + \frac{\sigma_{ult} - \sigma_{unl}}{\exp \left[\left(\frac{\log N}{\alpha} \right)^\beta \right]} \quad \text{with}$$

Ultimate Delamination Stress σ_{ult}
 Delamination Endurance Limit σ_{unl}
 Curve parameter α
 Curve parameter β

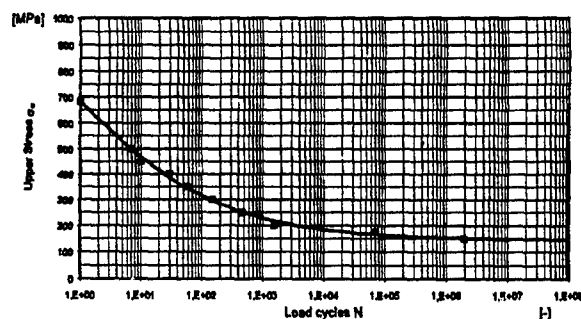


Figure 13: S/N-Curve for Delamination Strength of Unidirectional E-Glass/913

The relation between the stress σ_{II} and the energy release rate G_{II} with the specific parameters of the tested specimen reads:

$$G_{II} = \frac{1}{4} \cdot \frac{\sigma^2}{E} \cdot \frac{h \cdot t}{h - t} \quad \text{with}$$

Young's modulus $E = 41.5 \text{ GPa}$
 Specimen thickness $h = 1.25 \text{ mm}$
 Thickness of interrupted plies $t = 0.25 \text{ mm}$

The delamination growth rate was determined for materials widely used in the helicopter structures of ECD. The logarithmic linear relationship between the delamination growth rate da/dN and the energy release rate G_{II} in the range of stable delamination growth was derived from the test results. The range of stable delamination growth is bounded by the threshold value of G_{IIth} and the critical value G_{IIc} . Below G_{IIth} there is no crack propagation and above G_{IIc} the crack grows instantaneously.

$$\frac{da}{dN} = c \cdot G_{II\max}^n$$

with c and n being material constants describing the position and the slope of the curve.

Figure 14 shows the delamination growth rates versus energy release rate for E-Glass/913, carbon T300/913 and R-Glass/913 UD prepreg materials. In general it can be deduced from the gradient of the curves that materials with higher stiffness show more sensitivity of the crack propagation velocity against increasing cyclic energy release rate.

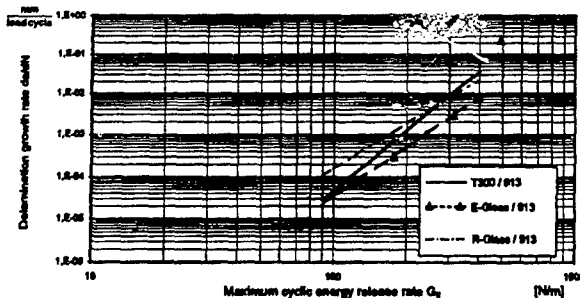


Figure 14: Delamination Growth Rate da/dN versus Energy Release Rate G_{II}

Figure 15 which is taken from [12] shows the comparison of the carbon fiber materials T300/914C and M40/Code69. Here this trend can be seen more clearly due to the higher difference in modulus between the two fiber types. In addition a difference in the threshold and critical value of G_{II} is obvious. The higher the modulus is, the higher is the threshold and the lower is the critical value of G_{II} . That is, the band between the threshold and the critical value of G_{II} becomes narrower. Thus the endurance limit comes closer to the static strength with increasing stiffness of the material. This effect can also be observed in the fatigue curves of high modulus carbon fibers.

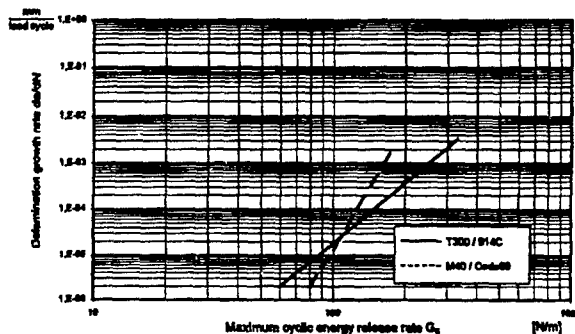


Figure 15: Delamination Growth Rate da/dN versus Energy Release Rate G_{II} according to [12]

In Table 6 the test results for the critical energy release rate G_{IIc} are listed for E-Glass/913, T300/913 and T300/M18. In addition the value for E-Glass/913 with an additional layer of adhesive between the continuous and interrupted layers is shown. This intermediate bonding layer ameliorates the critical value substantially. This effect can be easily transferred into design solutions to improve areas prone to delamination. The comparison of the two resin systems for the carbon laminates emphasizes the importance of the resin properties for the delamination strength of fiber composite components.

Table 7 summarizes the curve parameters of the delamination S/N curves and the crack propagation curves of E-Glass/913, R-Glass/913 and T300/913. The links between the both types of curves are the static delamination strength σ_{ult} and the

delamination endurance limit σ_{unl} which can be transformed into the critical and threshold value G_{IIc} and G_{IIth} respectively.

Table 6: Critical Energy Release Rate G_{II} for Several Unidirectional Composites

Unidirectional Material	Young's Modulus E [GPa]	H [mm]	T [mm]	Critical Energy Release Rate G_{IIc} [N/m]
E-Glass/913	41.3	1.3	0.26	914
E-Glass/913 with Bonding Layer	40.3	1.4	0.26	1944
T300/913	126.4	1.3	0.26	791
T300/M18	133.1	1.3	0.26	958

Table 7: Delamination Onset and Propagation Curve Parameters

Material	σ_{ult} [MPa]	σ_{ult} [MPa]	α [-]	β [-]	c [*]	n [-]
T300/913	315	884	3.166	1.496	2.852	4.793
E-Glass/913	149	650	1.772	1.174	0.287	3.915

* Dimension of c : $[(m/N)^n \cdot mm/load\ cycle]$

6. BASIC STRUCTURAL BEHAVIOUR

For the blade design, the cross section characteristics were calculated at various radius stations with the help of a two-dimensional finite element (FE) program. This ECD own code computes the six different stiffnesses corresponding to the forces and moments in the three coordinate directions. Additionally it also calculates the normal and shear stress distributions for any load combination. Figure 16 shows a typical FE modelization of the airfoil section.



Figure 16: Cross Section FE Model of the Airfoil Section

This FE analysis yields good results. However, it assumes that the cross section remains constant over a greater length.

In order to determine additional stresses e.g. due to strong cross section variations or special load introduction areas, such as the glass fiber lug the fixation with the help of a titanium fitting, are treated by special tools and calculation procedures.

A critical load situation of the BK 117 root area is the dynamic lead-lag motion. The interaction between the glass fiber composite loop and the titanium fitting due to centrifugal force and lead-lag-moment was modelled in finite elements. The stresses in the composite loop were calculated with the program system MARC in an iterative process. The contour of the titanium fitting was optimised in order to reduce stress peaks in the loop.

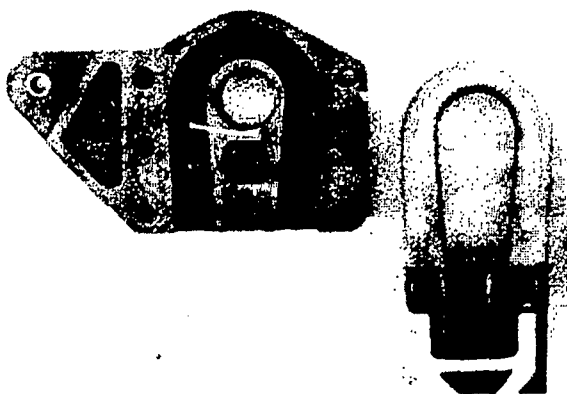


Figure 17: BO105/BK117 Blade Root Glass Fiber Loop and Titanium Fitting

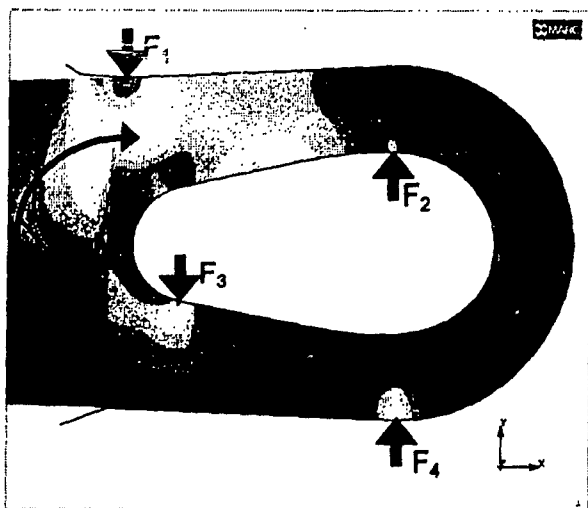


Figure 18: Transverse Stresses in the Loop due to Lead-Lag Bending Moment

For the Flexbeam of the EC 135 a three-dimensional Finite Element (FE) model was developed in order to determine additional stresses e.g. due to strong cross section variations.

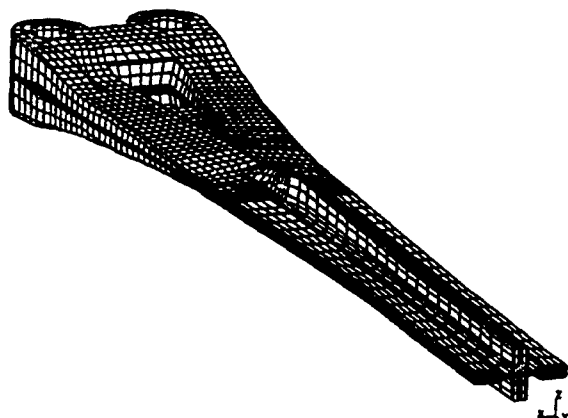


Figure 19: Three-Dimensional FE Model of the Prototype Flexbeam

Furthermore flaws, which had been detected in component tests, were introduced into the three-dimensional FE-model in

order to determine the criticality to the overall strength behaviour of the blade root [15].

7. DYNAMIC STRENGTH COMPONENT TESTING AND DEMONSTRATION OF LIMIT LOAD CAPACITY

It is not possible to test a complete blade realistically at all possible load combinations in a testing machine. Therefore the blade was subdivided into several components each of them being tested under its critical load conditions. For each test type several specimens with intrinsic, manufacturing and impact damages were tested at different load levels. The impact energy for flexbeam and control cuff was 25 J. This means a 2.5 kg impact mass falling from 1 m height.

For the static ultimate load tests the influence of high temperature and moisture had to be taken into account according to the 'Special Condition'. The strength degradation was determined by coupon tests, see chapter 4. The static component tests were then performed at room temperature with loads increased by the hot/wet degradation factors. The maximum loads were simultaneously applied to cover the worst case possible.

After the fatigue tests residual strength tests had to be performed. Limit load capacity was proven there, also including load amplification factors to simulate hot/wet conditions.

Table 8 summarises the process for the component tests taking into account the requirements of the 'Special Condition'. These tests were the basis for the life calculations.

Table 8: Process for the (Sub-)Component Tests

- | |
|--|
| 1. Component specimens |
| - Specimens with intrinsic, manufacturing and impact damages |
| 2. Tests |
| - Separate component tests for critical areas |
| - Constant amplitude tests at different load levels |
| - Test monitoring |
| - Documentation of: Type of damage |
| Damage begin |
| Size |
| Location |
| Growth rate |
| 3. Residual strength test with predamaged specimens after fatigue test |
| - Proof of Limit Load capacity |
| - Load amplification factor to simulate hot/wet conditions |

Figure 20 shows a bending specimen of the flexbeam in its upper and lower test position. It is pretensioned by a centrifugal force of about 150 kN and simultaneously loaded by flapping and lead-lag moments (number 1 of the flexbeam tests from above). At the left side the blade attachment area is clamped into a fork simulating the rotor hub. At the right side two hydraulic cylinders introduce the maximum transverse forces and flapping and lead-lag moments simultaneously. This test mainly simulates the load conditions between blade attachment and 'flapping hinge'.

During the development phase the flexbeam was continuously improved and the S/N-curve concerning bending could be raised by about 20%.

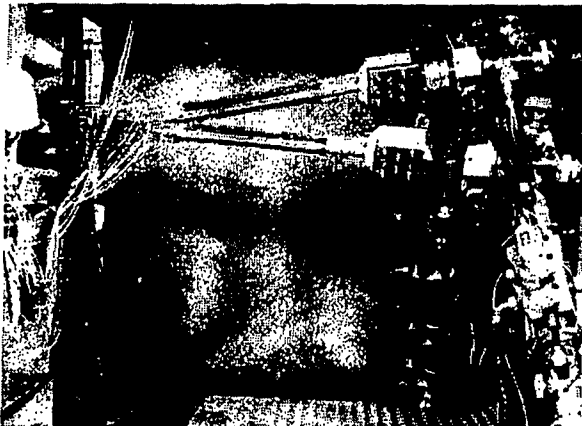


Figure 20: Flexbeam Specimen Loaded by Bending Moments and Centrifugal Force

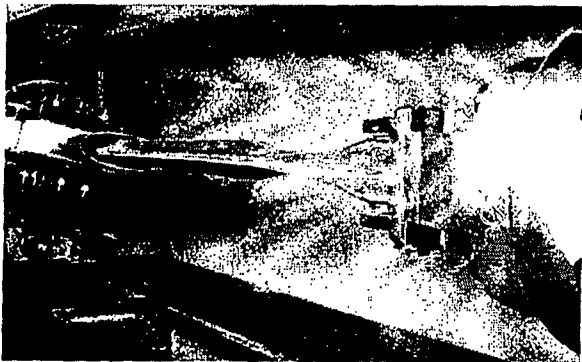


Figure 21: Flexbeam Unloaded

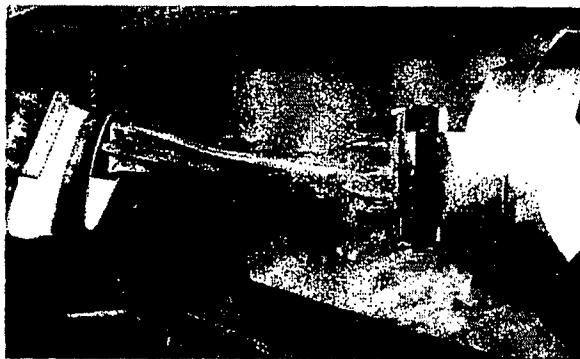


Figure 22: Flexbeam Loaded by Centrifugal Force and Twisted by 100°

The torsional capability of the flexbeam was proved in another test sequence. Figure 21 shows the specimen unloaded. The cuff is almost completely removed. At the right side the blade attachment area of the flexbeam is clamped. (To the left it is followed by the flat 'flapping hinge' and the torsional element with its slit cruciform cross section.) In Figure 22 the specimen is pretensioned by a centrifugal force of 150 kN and is twisted by 100°. This means a torsional angle of 2°/cm length of the torsional element. The specimen showed no failure, the

test was only limited by the capacity of the testing machine. This test proved the outstanding qualities of the EC135 flexbeam.

8. SUMMARY

During the last decades the former helicopter division of MBB and now Eurocopter Deutschland has consequently developed the main rotor systems towards simplification, improved reliability, increased life, lower weight and reduced service and maintenance costs. It started with the hingeless rotor of the BO105 and continued to the bearingless rotor of the EC135. However, this became only possible by using the outstanding qualities of glass fiber composites with regard to strength and flexibility.

As the certification authorities demand for an improved damage tolerant behaviour, especially for dynamically loaded structures, basic damage tolerance material data were studied. The basic delamination growth data for several unidirectional fiber/epoxy combinations were determined with the help of TCT test specimens. The gained database allows sizing of dynamically loaded flexbeams. The load case of flap bending corresponds to the mode II whereas the torsional load case corresponds to mode III. The outstandingly low crack growth behaviour of composite materials and improved methods of quality assurance, such as computed tomography (CT), reduce life cycle costs and improve the structural safety of helicopters remarkably.

REFERENCES

- [1] Huber, H., and Schick, C.,
'MBB's BO108 Design and Development',
46th Annual Forum & Technology Display of the
American Helicopter Society, Sheraton Washington
Hotel, Washington D.C., 21-23 May 1990
- [2] Attlfellner, S.,
'Eurocopter EC135 Qualification for the Market',
22nd European Rotorcraft Forum, Brighton, UK.,
17-19 September 1996
- [3] Bansemir, H., and Mueller, R.,
'The EC135 - Applied Advanced Technology',
AHS, 53rd Annual Forum, Virginia Beach, USA,
29 April - 1 May 1997
- [4] Pfeifer, K., and Bansemir, H.,
'The Damage Tolerant Design of the EC135 Bearingless
Main Rotor',
24th European Rotorcraft Forum, Marseilles, France,
15-17 September 1998
- [5] Och, F.,
'Fatigue Strength',
AGARDograph No 292, Helicopter Fatigue Design
Guide, Nov. 1983 ISBN 92-835-0341-4
- [6] Rauch, P., and Charreyre, A.,
'Damage - Tolerant Tail Rotor Blade for AS 332 L2 Su-
per Puma Helicopter'
19th European Rotorcraft Forum, 14-16 September
1993, Cernobbio (Como), Italy
- [7] Oster, R.,
'Computed Tomography as a Nondestructive Test
Method for Fiber Main Rotor Blades in Development,
Series and Maintenance',
23rd European Rotorcraft Forum, Dresden, Germany,
16-18 September 1997
- [8] Notzon, T.,
'Analyse und Versuche an geschäfteten Laminaten',
Diplomarbeit an der Universität der Bundeswehr
München / Eurocopter Deutschland 1993
- [9] Rapp, H.,
'Berechnung von Delaminationen in Aufdoppelungen
und Ausschäftungen',
ECD-DE133 (Internal Report) - 1993
- [10] Wisnom, M. R.,
'Delamination in Tapered Unidirectional Glass Fiber
Epoxy at Static Tension Loading',
Proc. AIAA Structures,
Structural Dynamics and Materials Conference,
Baltimore, April 1991, pp. 1162 - 1172
- [11] Sigh, G.C., and Paris P.C.,
'Stress Analysis of Cracks',
ASTM STP 381, p.60, 1985
- [12] Prinz, R., and Gädke, M.,
'Characterization of Interlaminar Mode I and Mode II
Fracture in CFRP Laminates',
Proc. Internat. Conf.: Spacecraft Structures and Me-
chanical Testing, Noordwijk, 1991
- [13] Cui, W. C., Wisnom, M. R., and Jones, M.,
'A Comparison of Fracture Criteria to Predict Delami-
nation of Unidirectional Glass / Epoxy Specimens with
Cut Central Plies',
5th Int. Conf. on Fiber Reinforced Composites,
Newcastle, March 1992
- [14] Murri, G. B., O'Brian, T. K., and Salpekar, S. A.,
'Tension Fatigue of Glass / Epoxy and Graphite / Epoxy
Tapered Laminates',
46th Annual AHS Forum, Washington D.C., May 1990
- [15] Boelingen, M., and Nawrath, C.,
'Bruchmechanische Analyse des Biege- und Drillstruk-
turelements des Hauptrotorblattes für einen Mehrzweck-
hubschrauber',
Diplomarbeit an der Universität der Bundeswehr
München / Eurocopter Deutschland 1995